Poultry Science

RNA N^6-methyladenosine profiling reveals differentially methylated genes associated with intramuscular fat metabolism during breast muscle development in chicken

Baojun Yu, Jiamin Liu, Zhengyun Cai, Haorui Wang, Xiaofang Feng, Tong Zhang, Ruoshuang Ma, Yaling Gu, and Juan Zhang[1]

College of Animal Science and Technology, Ningxia University, Yinchuan 750021, China

ABSTRACT Intramuscular fat (**IMF**) is an important indicator for determining meat quality, and IMF deposition during muscle development is regulated by a complex molecular network involving multiple genes. The N^6-methyladenosine (**m^{6}A**) modification of mRNA plays an important regulatory role in muscle adipogenesis. However, the distribution of m^{6}A and its role in IMF metabolism in poultry has not been reported. In the present study, a transcriptome-wide m^{6}A profile was constructed using methylated RNA immunoprecipitation sequence (**MeRIP-seq**) and RNA sequence (**RNA-seq**) to explore the potential mechanism of regulating IMF deposition in the breast muscle based on the comparative analysis of IMF differences in the breast muscles of 42 (group G), 126 (group S), and 180-days old (group M) Jingyuan chickens. The findings revealed that the IMF content in the breast muscle increased significantly with the increase in the growth days of the Jingyuan chickens ($P < 0.05$). The m^{6}A peak in the breast muscles of the 3 groups was highly enriched in the coding sequence (**CDS**) and 3′ untranslated regions (**3′ UTR**), which corresponded to the consensus motif RRACH. Moreover, we identified 129, 103, and 162 differentially methylated genes (**DMGs**) in the breast muscle samples of the G, S, and M groups, respectively. Functional enrichment analyses revealed that DMGs are involved in many physiological activities of muscle fat anabolism. The m^{6}A-induced ferroptosis pathway was identified in breast muscle tissue as a new target for regulating IMF metabolism. In addition, association analysis demonstrated that *LMOD2* and its multiple m^{6}A negatively regulated DMGs are potential regulators of IMF differential deposition in muscle. The findings of the present study provide a solid foundation for further investigation into the potential role of m^{6}A modification in regulating chicken fat metabolism.

Key words: Jingyuan chicken, intramuscular fat, N^6-methyladenosine, MeRIP-seq, transcriptional regulation

2023 Poultry Science 102:102793
https://doi.org/10.1016/j.psj.2023.102793

INTRODUCTION

It is gradually becoming recognized that the high-intensity selection of poultry growth rate and meat production performance can cause a significant decrease in muscle quality to a certain extent. Intramuscular fat (**IMF**) can improve the flavor, tenderness, and juiciness of meat and is an important indicator of muscle quality (Frank et al., 2016). IMF was mainly deposited on the myoepimysium and myofascicular membrane in the muscles. It is a complex physiological process in which myocytes and adipocytes grow together, interact, and are regulated by multiple transcription factors and signaling pathways (Hocquette et al., 2010). However, in addition to specific factors regulating the transcriptional regulation of IMF metabolism, epigenetic modifications are involved in multiple biological processes of adipocyte differentiation (Song et al., 2020).

N^6-methyladenosine (**m^{6}A**) is the most common methylation modification observed in eukaryotic RNA, representing a novel mode of post-transcriptional gene regulation (Roundtree et al., 2017; Frye et al., 2018; Yang et al., 2018). m^{6}A methylation is a reversible modification process dynamically regulated by a series of methyltransferase complexes, m^{6}A-binding proteins, and demethylase activity (Yang et al., 2018). m^{6}A modification is involved in almost all RNA metabolic processes in the regulation of gene expression (Zhao et al., 2017), thereby playing an important role in biological activities such as tissue growth and development, cell differentiation (Frye et al., 2018; Lee et al., 2019), and lipid metabolism (Song et al., 2020). m^{6}A modifications

Received March 14, 2023.
Accepted May 15, 2023.

[1]Corresponding author: zhangjuannxy@nxu.edu.cn

have been involved in fat anabolic processes by regulating transcription factors and adipose tissue-specific gene expression. The demethylase *FTO* is required for preadipocyte differentiation, and m^6A modification mediated by it acts as a switch to promote adipogenesis (Zhao et al., 2014; Merkestein et al., 2015). In contrast, increased levels of m^6A mediated by the methyltransferase *METTL3* inhibited fat deposition (Wang et al., 2015; Song et al., 2020). AMPK reduces the level of m^6A during skeletal muscle cell differentiation via *FTO*-dependent demethylation, affecting fat accumulation in skeletal muscle cells (Wu et al., 2017). Despite extensive research into the relationship between m^6A modification and adipogenesis in recent years, its functional mechanism in IMF metabolism in poultry has not been fully described.

Jingyuan chicken is an excellent local chicken breed resource in the Catalogue of Chinese Livestock and Poultry Genetic Resources, with characteristics such as rough feeding resistance, strong adversity resistance, and delicious meat. It has developed its own distinct meat-quality genetic law. The present study revealed that the IMF content in the breast muscles of Jingyuan chickens increased significantly during their growing period, sexual maturity, and market age. Given the importance of m^6A methylation modifications in adipogenesis, we analyzed and compared the m^6A methylation patterns during breast muscle development in the Jingyuan chicken and investigated the functions of m^6A-modified genes and their potential mechanisms for regulating IMF metabolism. The findings of the present study provide a basis for determining the role of m^6A modification in regulating chicken IMF metabolism.

MATERIALS AND METHODS

Ethical Statements

The animal experiments in the present study were carried out in accordance with the Regulations on Administration of Animals Used as Subjects of Experiments issued by the State Council of China. They were approved by the Experimental Animal Welfare and Ethics Review Committee of Ningxia University (Ningxia, China).

Animal and Tissue Collection

Jingyuan chickens were provided by a national-grade breeding farm in Pengyang County, Ningxia. All chickens were hatched in the same batch, with the same genetic background and level of feeding management. Ten white-feathered hens of comparable body weight were selected for the growing period (42-days old), sexual maturity (126-days old), and market age (180-days old) and weighed and slaughtered after 12 h of fasting. The breast muscle tissues were then rapidly separated on both sides, and part of the tissue samples was snap-frozen in liquid nitrogen and stored at −80°C, while the other part was used to determine the fat content.

Fat Content Determination

The fat content of breast muscle was determined using the national standard "National standard for food safety: determination of fat in food" (GB 5009. 6-2016). The 3 to 5 g mixed samples were weighed and baked in a desiccator until completely dry. The samples were then extracted for 6 to 10 h on a Soxhlet extractor with anhydrous ether as the solvent, and the residue obtained after solvent recovery was fat in the tissue.

RNA Extractions and Real-Time Quantitative PCR

Total tissue RNA was extracted using RNAiso Plus (Takara, Dalian, China) as directed by the manufacturer. Then, cDNA was synthesized via reverse transcription using the PrimeScript^{RT} Reagent Kit (Perfect Real Time; Takara, Dalian, China). Table S1 presents the primer sequences. The quantitative PCR was performed on a CFX96 real-time PCR detection system (Bio-Rad, Hercules, CA) according to the instructions of the SYBR$^{@}$ Green Premix Pro Taq HS qPCR Kit (Accurate Biotechnology (Hunan) Co., Ltd., ChangSha, China) with β-actin as the internal reference. The relative mRNA expression was calculated using $2^{-\triangle\triangle Ct}$ methods.

Methylated RNA Immunoprecipitation Library Construction and Sequencing

The total RNA of each of the 5 breast muscle tissues of Jingyuan chickens aged 42 d (group G), 126 d (group S), and 180 d (group M) was selected as sequencing samples in the study. First, poly(A)-containing RNA was isolated from total RNA using Dynabeads Oligo (dT) (Thermo Fisher, Waltham, CA) and divided into short fragments of 50 to 100 nt under high temperature and magnesium ions (NEBNext Magnesium RNA Fragmentation Module, NEB, Ipswich, MA). The fragmented RNA was divided into 2 parts: one for direct reverse transcription synthesis of the transcriptome sequencing library and the other for placing in immunoprecipitation (**IP**) buffer (50 mM Tris-HCl, 750 mM NaCl, and 0.5 Igepal CA-630) containing m^6A antibody (Synaptic Systems, Goettingen, Germany), mixed with immunomagnetic beads (Dynabeads Antibody Coupling Kit; Thermo Fisher, CA) and incubated at 4°C for 2 h. The resulting IP products were synthesized as single-stranded cDNA using SuperScript II reverse transcriptase (Invitrogen, Waltham, CA). dUTP (Thermo Fisher, CA) was added, and DNA polymerase I (NEB) and RNase H (NEB) was used to synthesize double-stranded cDNA and an A was then added to each end of the double-stranded DNA. The 180 to 220 bp fragment was screened with magnetic beads and enriched by PCR to produce the final cDNA library. Finally, double-end 150-bp sequencing was performed on the Illumina Novaseq 6000 platform (LC-Bio Technology CO., Ltd., Hangzhou, China).

Bioinformatics Analysis

The raw sequences were all deposited in the NCBI database Sequence Read Archive under the accession number PRJNA898123. The raw data obtained from sequencing were saved in fastq format. The raw reads of IP and input samples were first filtered using fastp software (Chen et al., 2018). The high-quality valid reads were obtained by removing the adapter, repetitive, and low-quality sequences. Valid reads were compared with the *Gallus gallus* reference genome (GRCg6a_v101) using HISAT2 (Kim et al., 2015) to compare and obtain detailed read information. The R package exomePeak2 was used to analyze data such as the position and length of the peak on the genome (Meng et al., 2014). After testing by the Poisson distribution model on the candidate peak region with genomic reads, the region with a P value <0.05 was considered a peak. The above-mentioned m^{6}A peak was then annotated using ANNOVAR (Wang et al., 2010). MEME2 (Bailey et al., 2009) and HOMER (Heinz et al., 2010) were used to identify the motifs associated with peaks in each group of samples, and data such as the P value and percentage of targets of each motif were obtained. Gene expression levels in the 15 samples were analyzed using StringTie software (Pertea et al., 2015), which calculated Fragments Per Kilobase of the exon model per Million mapped reads (**FPKM**) for each gene. The R package edgeR (Robinson et al., 2010) was then used for differential expression analysis between the 2 groups. The $|\log_2(\text{fold change})| \geq 1$ and P value <0.05 were used as thresholds to determine the differentially expressed genes (**DEGs**) between groups. To investigate the relationship between m^{6}A methylation and gene expression abundance, we merged differential peaks with DEGs, and genes with one or more m^{6}A peaks were considered differentially methylated genes (**DMGs**). The Gene Ontology (**GO**) (http://www.geneontology.org/) function and the Kyoto Encyclopedia of Genes and Genomes (**KEGG**) (http://www.kegg.jp/kegg) pathway enrichment analysis were used to determine the functional role of DMGs and DEGs.

Statistical Analysis

GraphPad Prism (version 8.0.2) software performed data analysis and visualization. Data were expressed as the mean ± standard error of the mean (**SEM**). An unpaired 2-tailed Student t test was used to compare differences between the 2 groups. One-way analysis of variance (**ANOVA**) was used to evaluate differences between multiple groups, followed by Tukey's multiple comparisons tests. Correlations were determined using Pearson correlation analysis. When the P value was less than 0.05, the results were statistically significant.

RESULTS

Fat Content in the Breast Muscles at 3 Developmental Stages

We measured the fat percentage in the breast muscles at 3 developmental stages to confirm the differences in fat content during Jingyuan chicken breast muscle development. The results revealed that the fat percentage in the breast muscle of Jingyuan chickens increased significantly with age (Table 1).

Table 1. Fat percentage in breast muscle at 3 developmental stages.

Ages	42-days old	126-days old	180-days old
Fat percentage (%)	0.39 ± 0.03^{A}	$1.14 \pm 0.08^{B,a}$	$1.64 \pm 0.20^{B,b}$

[AB]Different capital letters indicate extremely significant differences ($P < 0.01$).
[ab]Different lowercase letters indicate significant differences ($P < 0.05$).

Transcriptome-Wide Detection of m^{6}A Modification in the Breast Muscle of Jingyuan Chicken

In the present study, 15 IP libraries produced 32,808,986 to 54,128,964 raw reads, while input libraries produced 34,482,536 to 53,911,290 raw reads. To ensure the quality of the data analysis, low-quality reads in the raw reads were removed, yielding 31,416,218 to 52,623,496 valid reads with Q30 and GC contents greater than 91.59 and 47.97%, respectively (Table S2). In all samples, the number of valid reads compared to the *Gallus gallus* genome was more than 79.47% (Table S3), with unique mapped reads and multimapped reads averaging more than 62.07 and 18.66%, respectively (Figure 1A). The proportion of exon regions in IP and input libraries was the highest in the valid reads compared to the genome (Figure 1B). A genome-wide peak scan was then performed, and 18,015, 17,164, and 16,783 m^{6}A peaks with average lengths of 4,364 bp, 4,124 bp, and 4,616 bp were identified in group G, S, and M breast muscle samples, respectively. Figure 1C depicts the length distribution of m^{6}A peaks in the 3 sample groups. The m^{6}A peaks in groups G, S, and M corresponded to 10,250, 10,116, and 9,800 genes, respectively, with 76.27, 73.96, and 79.22% of genes having only 1 peak, and the proportion of genes having 2 or 3 peaks being relatively high, with only a few genes containing 4 or more m^{6}A peaks (Figure 1D).

Identification and Differential Analysis of the Genome-Wide m^{6}A Peak

The consensus motifs of the m^{6}A peak in groups G, S, and M (Figure 2A) were consistent with the classical m^{6}A motif RRACH (where R = A/G, A = m^{6}A, and H = A/C/G), further improving the credibility of the m^{6}A peak. The mRNA sequence was divided into 7 functional regions based on gene annotations and nonoverlapping segments to analyze the preferential location of the m^{6}A peak. The m^{6}A peak in the 3 groups of breast muscle was most enriched in a stop codon and coding sequence (**CDS**), followed by 3′ untranslated regions (**UTR**), and a few in the 5′ UTR, start codon and intron (Figure 2B). The relative positions of m^{6}A peaks in

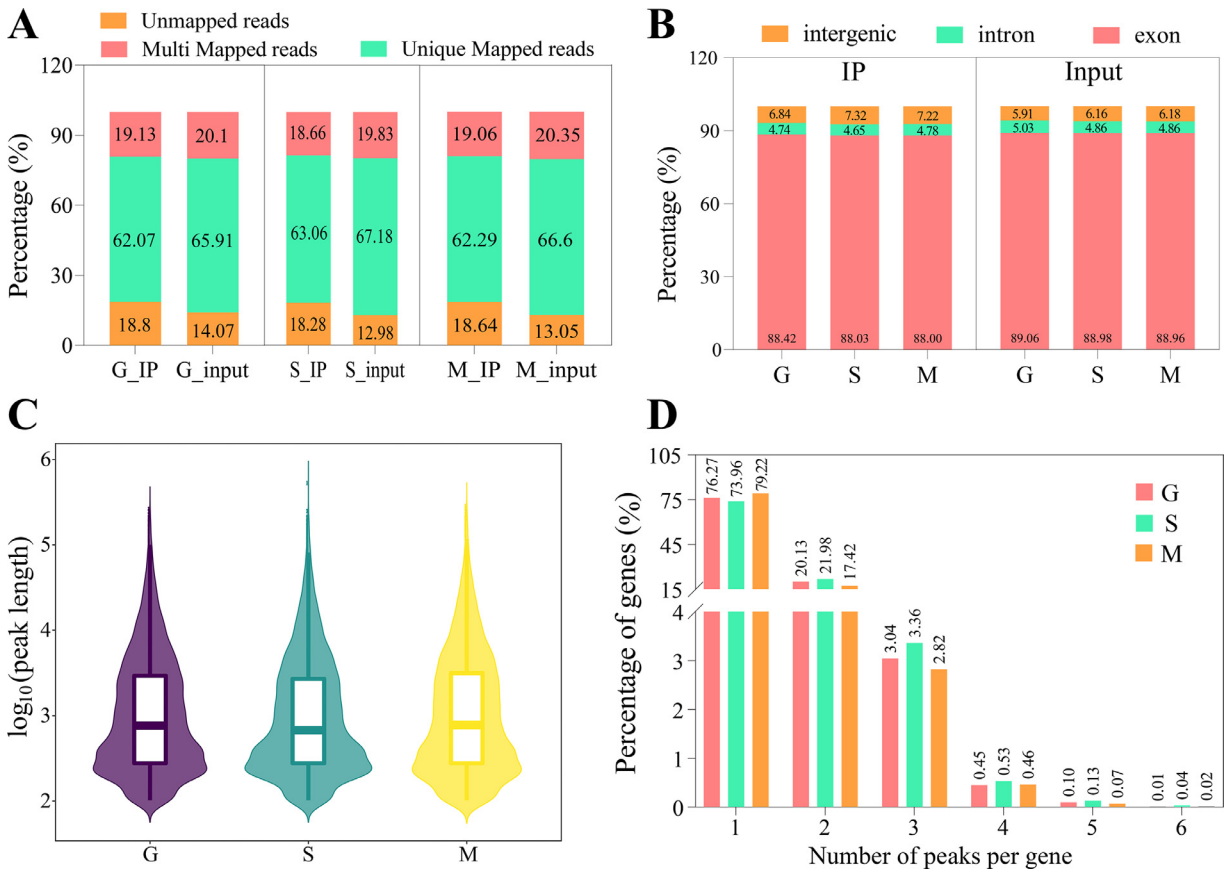

Figure 1. Methylation sequencing and m^{6}A peak identification of group G, S, and M breast muscle samples. (A) Comparison of read distribution in IP and input samples. Unique mapped reads: The number of reads can only be unique compared to a specific location in the genome. Multi-mapped reads: The number of reads that can be compared to multiple locations in the genome. (B) Distribution of valid reads compared to exon, intron, and intergenic regions of the reference genome. (C) Length distribution of m^{6}A peaks in groups G, S, and M. (D) The percentage of m^{6}A-methylated genes with various m^{6}A peaks.

mRNA revealed that the 3 groups of peaks were highly enriched in the CDS and 3′ UTR (Figure 2C). Moreover, m^{6}A methylation was extensively modified in group G, S, and M breast muscles, and the distribution trend of m^{6}A methylation sites was consistent, with 3 chromosomes, chr1, chr2, and chr3 having the most peaks (Figure 2D).

Furthermore, we compared the abundance of m^{6}A peaks in breast muscle samples from groups G, S, and M. Compared to group G, group S had 713 hypermethylated and 419 hypomethylated peaks ($P < 0.05$, fold change >1.5) (Figure 2E, Table S4). Group M had 393 hypermethylated and 1,490 hypomethylated peaks compared to group S (Figure 2F). While group M had 458 hypermethylated and 807 hypomethylated peaks compared to group G (Figure 2G). In conclusion, the most significant difference in m^{6}A methylation was identified between the 126 d and 180 d of breast muscles of the Jingyuan chickens, and the number of hypomethylated m^{6}A peaks was significantly higher than that of hypermethylated m^{6}A peaks.

Differential m^{6}A peaks were then analyzed overlapping in the 3 comparison groups to investigate further the m^{6}A methylation sites that were consistently modified during breast muscle development. Figure 2H indicates only 5 shared differential peaks in the 3 comparison groups located on chromosomes chr16, chr15, chr1, chr4, and chr1, respectively. Based on David's (https://david.ncifcrf.gov/) functional enrichment analysis, 80 genes continuously modified by m^{6}A during breast muscle development were significantly enriched into multiple functional terms (Figure 2I), including receptor transactivation, adenylate cyclase-activating adrenergic receptor signaling pathway, regulation of GTPase activity, notch signaling pathway, positive regulation of MAPK cascade, myosin complex, and focal adhesion (Table S5).

Screening and Functional Enrichment Analysis of Intergroup DEGs

The transcriptome analysis of mRNA expression patterns in breast muscle tissues of groups G, S, and M was performed. In the S vs. G comparison group, 906 DEGs were identified, with 477 being upregulated and 429 being downregulated (Figure 3A, Table S6). GO analysis revealed that DEGs were significantly enriched in signal transduction, cell proliferation regulation, and positive regulation of gene expression as well as molecular functions such as actin binding, chemokine activity, and glutathione transferase activity (Figure 3D). KEGG analysis demonstrated that DEGs were significantly enriched in several lipid anabolism-related

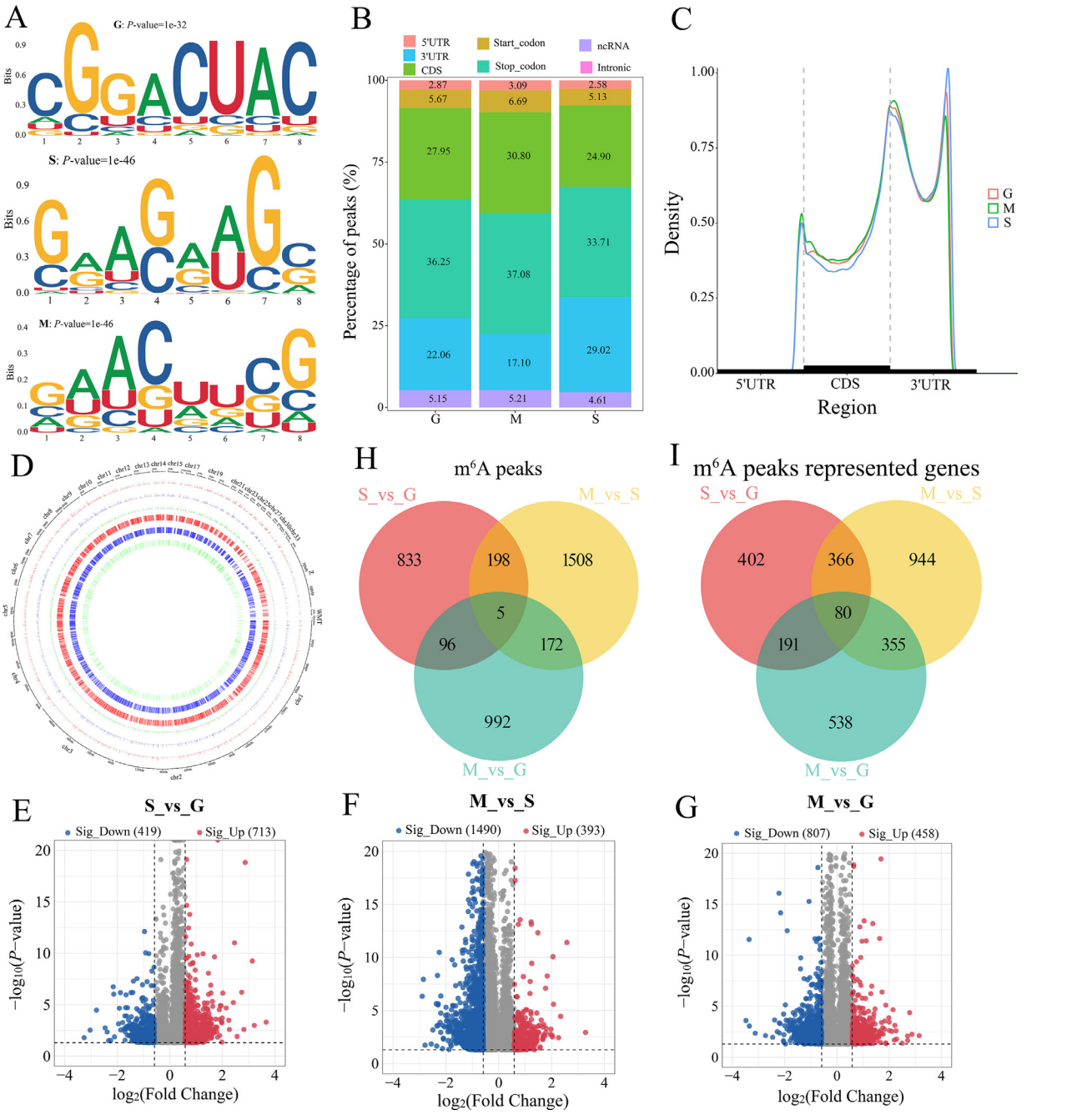

Figure 2. m^{6}A methylation profiles of Jingyuan chicken breast muscle at 3 key developmental stages. (A) Consensus motif of the m^{6}A peak in breast muscles of groups G, S, and M. (B) Frequency of m^{6}A peak distribution in 7 nonoverlapping functional regions in groups G, S, and M. (C) m^{6}A distribution peaks across transcripts divided into 3 segments: 5′ UTR, CDS, and 3′ UTR. (D) The overall distribution of m^{6}A methylation sites in the Jingyuan chicken genome. The circles from outside to inside represent the calling peak of the G (red), M (blue), and S (green) groups, and the gene expression results of the G (red), M (blue), and S (green) groups, respectively. Volcano plot of differential peaks in the (E) S vs. G, (F) M vs. S, and (G) M vs. G groups. (H) The m^{6}A common difference peaks in all 3 comparison groups. (I) The genes represented by differential m^{6}A peaks in the 3 comparison groups.

pathways, including the adipocytokine signaling pathway, PPAR signaling pathway, and the insulin signaling pathway (Figure 3G). In the M vs. S group, 552 DEGs were identified, 353 upregulated, and 199 downregulated (Figure 3B, Table S6). Functional analysis revealed that DEGs were significantly enriched in GO terms such as cell adhesion, steroid hormone-mediated signaling pathway, actin binding, and cation transmembrane transport (Figure 3E). It was also significantly enriched for focal adhesion, ECM-receptor interaction, the adipocytokine signaling pathway, glycerophospholipid metabolism, and the fatty acid biosynthesis signaling pathway (Figure 3H). In the M vs. G group, 1,148 DEGs were identified, with 674 being upregulated and 474 being downregulated (Figure 3C, Table S6). GO analysis demonstrated that DEGs were mainly involved in cell adhesion, proteolysis, cytokine-mediated signaling pathways, and molecular functions such as calcium ion binding, actin filament binding, and serine-type endopeptidase inhibitor activity (Figure 3F). DEGs were significantly enriched in several KEGG pathways, including ECM-receptor interaction, MAPK signaling

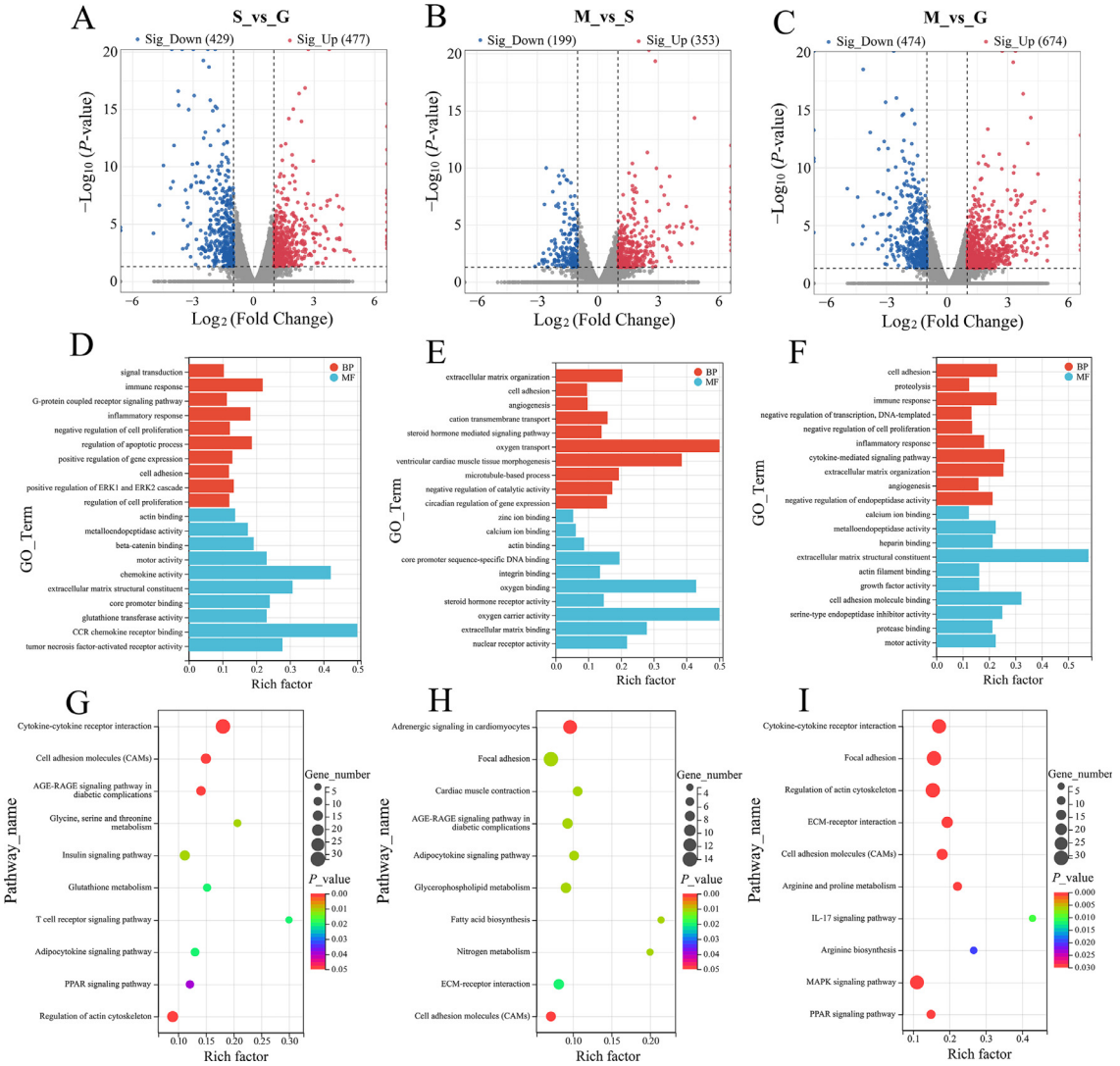

Figure 3. Identification and functional analysis of DEGs between breast muscles of groups G, S, and M. Volcano plot of DEGs in the (A) S vs. G, (B) M vs. S, and (C) M vs. G groups. GO functional enrichment results of DEGs in the (D) S vs. G, (E) M vs. S, and (F) M vs. G groups. The top 10 terms with the highest number of genes significantly enriched in biological processes (BP) and molecular functions (MF). KEGG pathway enrichment results of DEGs in the (G) S vs. G, (H) M vs. S, and (I) M vs. G groups. Display 10 signaling pathways significantly enriched in DEGs and associated with IMF anabolism.

pathway, PPAR signaling pathway, IL-17 signaling pathway, and arginine biosynthesis, which is widely involved in fat synthesis and metabolism (Figure 3I). The visualization of the Venn map revealed 39 genes of continuous differential expression (Figure S1A) during the breast muscle development of the Jingyuan chicken, of which 15 were continuously downregulated, and 18 were upregulated, while the 6 DEGs increased at first and then decreased (Figure S1B). Based on the identified DEGs in the IMF, the findings revealed various enriched pathways in adipocytokine interactions, fatty acid anabolism, amino acid metabolism, glucose homeostasis, and energy activity.

Association Analysis of mRNA-seq and m^{6}A-seq

We identify key DMGs that regulate IMF-specific deposition by correlating the intergroup difference peak with DEGs. There were 70 hypermethylated DMGs (29 mRNAs upregulated and 41 downregulated) and 59 hypomethylated DMGs (33 mRNAs upregulated and 26 downregulated) in the S vs. G comparison group (Figure 4A, Table S7). After identifying that DMGs were significantly enriched in the PPAR signaling pathway, ferroptosis, and fatty acid metabolism pathways (Figure 4D), we screened and identified the roles of *FABP4, EHHADH, PLIN5, HACD4, STEAP3*, and *HMOX1* in the lipid metabolism regulation. There were 19 hypermethylated DMGs (14 mRNAs upregulated and 5 downregulated) and 84 hypomethylated DMGs (63 mRNAs upregulated and 21 downregulated) in the M vs. S group (Figure 4B, Table S7). KEGG analysis revealed that DMGs were significantly enriched in arginine and proline metabolism, focal adhesion, and ECM-receptor interaction pathways (Figure 4E). The *SPP1, CHAD, HOGA1*, and *ARG2* genes regulated by them were associated with adipogenesis-related processes. There were 55 hypermethylated DMGs (37 mRNAs

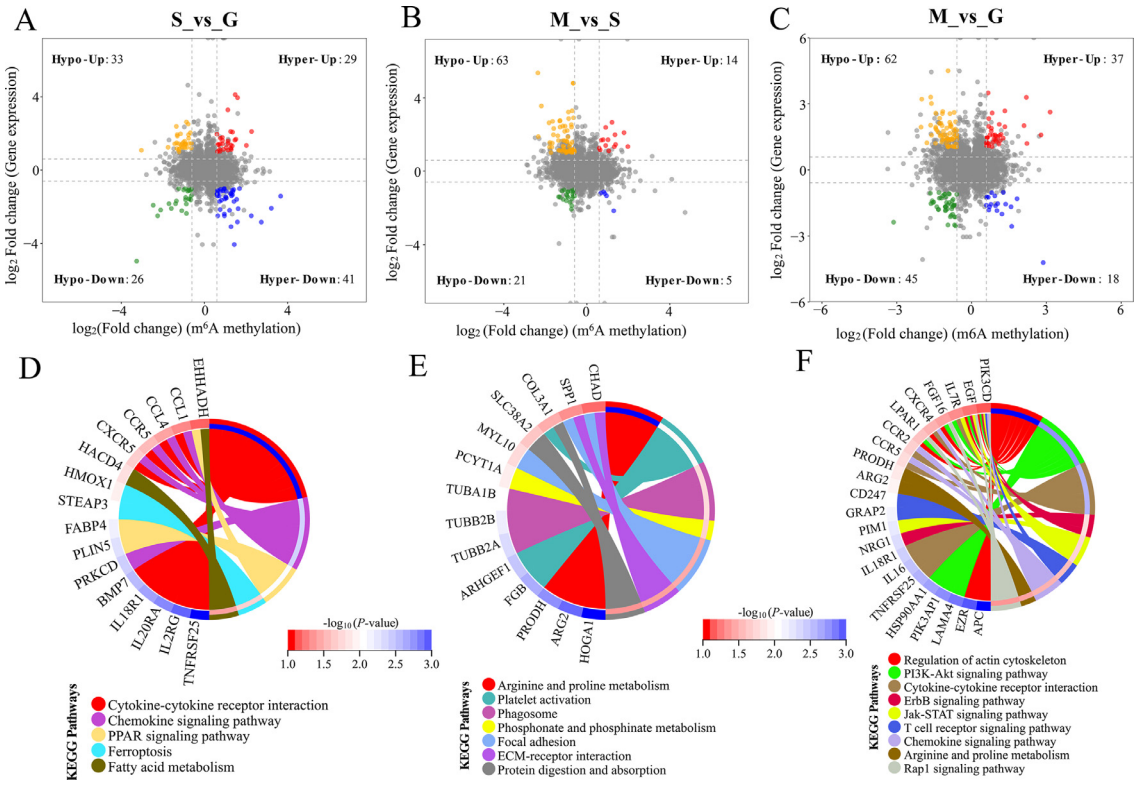

Figure 4. Association analysis of differential peaks and DEGs in breast muscle of the G, S, and M groups. Distribution of genes with significant changes in both m^{6}A methylation levels and gene expression in the (A) S vs. G, (B) M vs. S, and (C) M vs. G groups. Hyper-up: m^{6}A peak and mRNA expression upregulation; Hyper-down: m^{6}A peak upregulation and mRNA expression downregulation; Hypo-up: m^{6}A peak downregulation and mRNA expression upregulation; Hypo-down: m^{6}A peak and mRNA expression downregulation. KEGG pathway of DMGs enrichment in the (D) S vs. G, (E) M vs. S, and (F) M vs. G groups.

upregulated and 18 downregulated) and 107 hypomethylated DMGs (62 mRNAs upregulated and 45 downregulated) in the M vs. G group (Figure 4C, Table S7). DMGs are involved in more signaling pathways at this stage, including actin cytoskeleton regulation, the PI3K-Akt signaling pathway, the T-cell receptor signaling pathway, and the Rap1 signaling pathway (Figure 4F). Furthermore, the annotated *LPAR1, FGF16, EGF*, and *IL7R* in these pathways may be functional genes for regulating fat anabolism in muscle.

In addition, we classified the differential m^{6}A peaks in the 3 comparison groups as hyper- and hypomethylated DMGs. We used GO analysis to further investigate the potential biological significance of m^{6}A methylation in muscle fat anabolic processes. In the S vs. G comparison group, hypermethylated DMGs were primarily associated with calmodulin binding, actin binding, protein kinase inhibitor activity, and the pyruvate biosynthetic process. G-protein coupled receptor binding, actin binding, and RNA polymerase activity were all functions of the hypomethylated DMGs. The hypermethylated DMGs in the M vs. S group were involved in fewer functional terms, primarily protein localization, protein kinase, and carbohydrate binding. Whereas the hypomethylated DMGs were involved in catalytic activity, metabolic process, lipopolysaccharide binding, and various energy metabolic activities. The M vs. G group hypermethylated DMGs were mainly associated with muscle activity and transcriptional activity regulation processes, such as actin binding, cell junction, and transcription coactivator activity. In contrast, the hypomethylated DMGs were related to various cellular metabolic and energy conversion processes, such as G-protein coupled receptor binding, enzyme activator activity, and glucose transmembrane transport (Table S7).

Functional Gene Screening and Identification

Further investigation of DMGs regulating IMF-specific deposition revealed that only *LMOD2* was consistently differentially expressed in the breast muscle at all 3 developmental stages (Figure 5A). String database (https://cn.string-db.org/) analysis demonstrated that *LMOD2* interacts with *CSRP3* and multiple myosin family proteins (*MYL2, MYBPC1*, and *UNC45B*) (Figure 5B), which can regulate myofiber development, muscle contraction, and actin binding. Consistent with the mRNA-seq results, real-time quantitative PCR (**RT-qPCR**) results confirmed that the mRNA expression levels of *LMOD2* in breast muscles at different developmental stages were significantly different (Figure 6).

m^{6}A methylation was negatively correlated with gene expression levels in these differentially m^{6}A-modified genes (Figure 5C). This is consistent with the aforementioned association analysis of differential peaks with

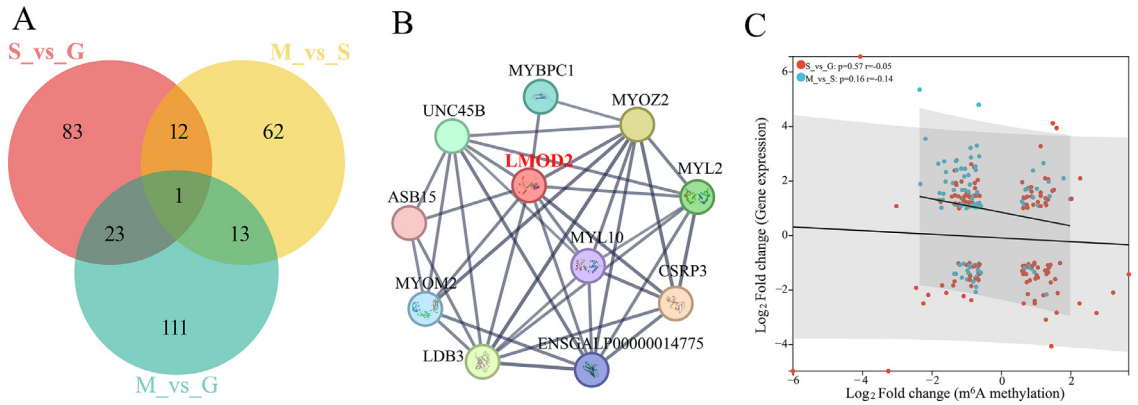

Figure 5. Identification of key DMGs in Jingyuan chicken breast muscles at different developmental stages. (A) DMGs common to the 3 comparison groups. (B) *LMOD2* protein interaction network analysis (edge confidence: 0.700). (C) Correlation analysis of m^6A methylation and mRNA expression in S vs. G group and M vs. S group.

DEGs, which indicates that hyper-down and hypo-up have more DMGs than hyper-up and hypo-down regulations (Figure 4A and B). In the S vs. G and M vs. S comparison groups, 12 stage-specific DMGs were identified, of which *HOGA1, MYH1F, LRRC66, TEKT1, DHX58, PPM1K, ANKRD2*, and *SACS* were m^6A-modified negative regulatory genes (Table 2). Functional investigations revealed that these 9 m^6A negatively regulated genes were associated with myoblast differentiation, RNA transcriptional regulation, protein kinase activity, catalytic activity, and mitochondrial and glucuronic acid catabolism processes.

RT-qPCR Validations of Differentially Expressed Genes

The mRNA expression levels of 9 of the DEGs shared by the 3 comparison groups were significantly different in breast muscles at different developmental stages

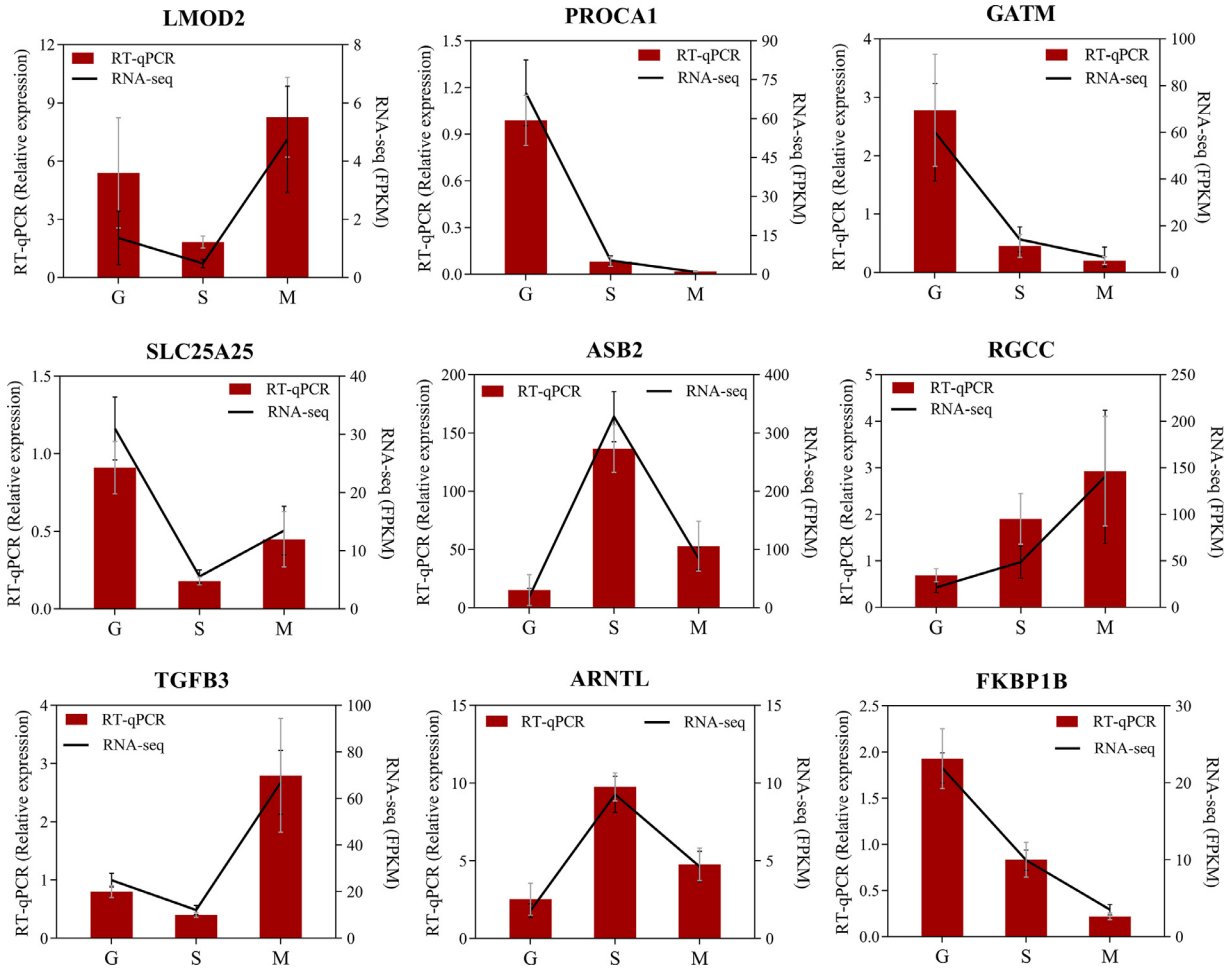

Figure 6. RT-qPCR validation of DEGs in breast muscle of groups G, S, and M.

Table 2. List of 13 genes with significant changes in both m^{6}A peak and mRNA expression in the S vs. G and M vs. S. comparison groups.

	S vs. G					M vs. S				
Gene name	Pattern	Peak. log_2fc	Peak. *P* value	Gene. log_2(fc)	Gene. *P* value	Pattern	Peak. log_2fc	Peak. *P* value	Gene. log_2(fc)	Gene. *P* value
HOGA1	Hyper-down	2.74	0.00	−2.84	0	Hypo-up	−2.36	0	5.36	0.00
MYH1F	Hyper-down	1.44	0.00	−4.06	0	Hypo-up	−1.73	0	1.02	0.01
LRRC66	Hyper-down	1.42	0.01	−1.72	0	Hypo-up	−1.78	0	1.56	0.00
TEKT1	Hyper-down	1.37	0.00	−1.17	0	Hypo-up	−1.15	0.01	1.37	0.01
DHX58	Hyper-down	1.34	0.00	−1.09	0	Hypo-up	−1.13	0	1.67	0.00
SLC25A15	Hyper-up	1.34	0.00	1.32	0	Hypo-down	−0.95	0.01	−1.37	0.00
LOC419333	Hyper-up	1.29	0.00	1.12	0.03	Hypo-down	−0.91	0.02	−1.43	0.01
PPM1K	Hyper-down	0.96	0.00	−2.4	0	Hypo-up	−0.75	0	2.54	0.00
ANKRD2	Hyper-down	0.82	0.00	−1.64	0	Hypo-up	−0.65	0.02	4.8	0.00
SACS	Hyper-down	0.63	0.01	−1.32	0	Hypo-up	−1.69	0	1.31	0.00
LMOD2	Hypo-down	−0.9	0.01	−1.49	0.04	Hypo-up	−0.71	0.01	3.3	0.00
GRIP2	Hypo-down	−1.09	0.02	−2.22	0	Hyper-up	1.36	0	1.98	0.01
TAL2	Hypo-down	−2.46	0.00	−1.92	0	Hyper-up	1.21	0.01	2.66	0.00

(Figure 6), which was consistent with the trend of RNA-seq, demonstrating the reliability of the sequencing results.

DISCUSSION

IMF is important for regulating muscle quality, and appropriate IMF deposition can significantly improve meat flavor and palatability (Katsumata, 2011; Frank et al., 2016). The amount of IMF deposition during the formation of animal meat varies significantly depending on species, sex, age, and tissue site (Chen et al., 2005; Cui et al., 2018; Cheng et al., 2021; Ou et al., 2022; Chen et al., 2023). It has been reported that changes in chicken quality occur primarily during the growing period, with IMF deposition increasing with age (Le Bihan-Duval et al., 2001; Cui et al., 2018; Li et al., 2020), which is consistent with the findings of the present study. However, with high-intensity genetic breeding selection, the relationship between muscle growth and development and meat quality has become gradually out of balance. Rapid muscle growth has resulted in histological and biochemical changes (Petracci and Cavani, 2012). That is, the ability of fat synthesis and metabolism in muscle decreased significantly. These differences were attributed to the complex regulatory processes that subjected adipocytes to multiple hormones and metabolic enzymes. Comparing the differences in IMF differential deposition at key developmental stages of Jingyuan chicken and determining the regulation mechanism of functional genes for IMF metabolism is thus an important step toward improving muscle quality.

m^{6}A methylation is the most common epigenetic modification of RNA transcription regulation in eukaryotes and is involved in gene expression regulation, cell differentiation, and metabolism-related biological processes (Dominissini et al., 2012; Luo et al., 2014). A transcriptome-wide assay for m^{6}A methylation in breast muscle tissues was performed in the present study at 42-, 126-, and 180-days old. Many m^{6}A methylation sites were present in the breast muscle at all 3 developmental stages, with these m^{6}A peaks primarily enriched in the CDS and 3′ UTR. This modification pattern is similar to that observed in rex rabbits, yaks, and pigs (Jiang et al., 2019; Zhang et al., 2021; Guo et al., 2022; Luo et al., 2022). However, species- and tissue-specific m^{6}A methylation patterns were identified in poultry studies. The m^{6}A peak in the breast muscle of Dingan goose embryos is enriched in the CDS and start codon (Xu et al., 2021). During chicken ovarian follicle selection, the m^{6}A mark is primarily localized in the start and stop codon regions (Fan et al., 2019). The m^{6}A methylation sites described above in the animals and tissues were consistent with the conserved motif RRACH. This modification feature has been validated in humans and mice (Dominissini et al., 2012; Meyer et al., 2012), and our findings support this. When these findings were combined with functional analysis, it was identified that genes consistently modified by m^{6}A in the 3 developmental stages can be involved in the regulation of GTPase activity, myosin complex, focal adhesion, and notch signaling pathways, implying a potential regulatory mechanism of m^{6}A methylation in IMF metabolism of the chicken breast muscle.

IMF deposition is a polygenic trait regulated by multiple gene networks directly or indirectly involved in fat anabolism (Cesar et al., 2015). The IMF content in the breast muscle of Jingyuan chickens increased from the beginning of the growth period to sexual maturity and up to marketable age. DEGs were widely expressed in breast muscles at various stages during this process. They participated in actin binding, protein kinase activity regulation, catalytic and transcriptional activity, glucose transport, carbon metabolism, and other biological functions. The functional pathways of DEGs enrichment in each group were examined, and the S vs. G group identified the adipocytokine signaling pathway (*ACSBG1, ADIPOR2, C1QTNF2*), PPAR signaling pathway (*APOA1, EHHADH, FABP4*), and insulin signaling pathway (*FOXO1, GCK, GRAPL*). Studies have shown that the insulin signaling pathway is important for glucose transport (Laukkanen et al., 2004; Davis et al., 2008). The energy generated by this process

protects adipocyte differentiation and metabolism (Saltiel and Pessin, 2002; Jiang et al., 2010). PPAR is a class of transcription factors from the nuclear receptor protein family, and its isoforms PPARα and PPARγ were widely expressed in liver and adipose tissue. They were involved in fat anabolism by regulating the expression of fatty acid transport and binding proteins (Soto-Avellaneda and Morrison, 2020). Moreover, the liver is not well developed. It has a limited capacity for fat synthesis during this period (Wang et al., 2021), which is consistent with the phenotype observed in our previous study, where no significant fat droplet deposition was seen in the liver tissue. Therefore, IMF deposition in the breast muscle from 42 to 126 d is primarily due to the synthesis of the breast muscle or the proliferation and differentiation of adipocytes in the breast muscle.

The DEGs in the M vs. S groups were significantly enriched in the adipocytokine signaling pathways (*RXRA* and *SOCS3*), glycerophospholipid metropolis (*AGPAT2, DGKH, ETNPPL*, and *GPAM*), fatty acid biology (*ACSL1* and *ACSL4*), ECM receiver interaction (*COL4A1, DIP2C*, and *THBS4*), and focal progression signal pathways (*MYL10, SPP1*, and *THBS4*). The protein composition of the extracellular matrix (**ECM**) is required for adipocyte growth and energy metabolism (Mariman and Wang, 2010). Focal adhesion is a protein complex connecting the ECM and actin cytoskeleton that plays an important role in skeletal muscle development and is the signaling center of cell growth and differentiation (Sastry and Burridge, 2000). The breast muscle develops more slowly after sexual maturation, resulting in reduced fatty acid oxidation capacity in breast muscle tissue. The liver's ability to synthesize fat has matured during this period. The liver regulates fatty acid synthesis through desaturation, elongation, and oxidation and thus plays a central role in lipid metabolism in poultry (Wang et al., 1984, 2006). The mitochondria-localized acyl-CoA synthetase long-chain family member 1/4 (***ACSL1/4***) primarily promotes fatty acid oxidation in the liver (Huh et al., 2020), and the extra-long-chain fatty acid elongase (***ELOVL***) family performs the same function (Chen et al., 2021). In the present study, *ACSL 1/4* and *ELOVL1* expression decreased significantly from 126- to 180-days old. Therefore, IMF deposition in breast muscle was mainly due to the increased ability to transport fat from the liver. In addition, increased IMF deposition can cause chickens to reach sexual maturation earlier (Zhao et al., 2007). Changes in hormone levels during sexual maturation, such as growth hormone receptor (**GHR**) deficiency that inhibits mitochondrial function promote adipocyte differentiation via the AMPK-PGC1α-PPAR signaling pathway, ultimately leading to fat deposition (Yang et al., 2022).

Notably, ferroptosis was significantly enriched during IMF deposition in the breast muscle. Ferroptosis is a novel cell death pathway caused by the massive accumulation of lipid peroxides induced by iron ions and reactive oxygen species (Jiang et al., 2021). Iron, an essential micronutrient, is required in skeletal muscle to maintain physiological functions (e.g., cell differentiation and growth) and energy metabolism. Transferrin receptor 1 (***TFR1***) deletion in muscle satellite cells resulted in dysregulated expression of the ferritin genes *HMOX1, SLC7A11*, and *ACSL4* and was accompanied by iron ion accumulation, unsaturated fatty acids synthesis, disruption in glutathione metabolism, and lipid peroxidation, all of which induce ferroptosis in skeletal muscle (Ding et al., 2021). Studies have demonstrated that amino acid and lipid metabolism are prerequisites for ferroptosis, and polyunsaturated fatty acids can promote ferroptosis via the peroxidation of specific membrane phospholipids (Stockwell, 2022). Heme oxygenase 1 (***HMOX1***) is a key inducer of intracellular heme degradation and iron production. Adding heme to human adipocytes during differentiation reduces intracellular lipid accumulation and significantly downregulates the expression of *ADIPOQ, FABP4, SLC2A4*, and *PLIN1* (Moreno-Navarrete et al., 2017). This is consistent with the findings in pigs (Park et al., 2015). The 6-transmembrane epithelial antigen of prostate 3 (***STEAP3***) is a ferric reductase that plays an important role in maintaining cellular iron homeostasis (Ohgami et al., 2005, 2006).

m^{6}A modifications are involved in various biological activities in eukaryotes, including RNA processing and metabolism, and are essential for regulating gene expression and functional cellular mechanisms. Based on this, emerging evidence reveals that m^{6}A modification and its regulators are essential in ferroptosis (Ruan et al., 2021; Shen et al., 2021). *HMOX1* and *STEAP3* m^{6}A methylation levels were significantly downregulated in the breast muscles from 42- to 126-days old in this study. Therefore, m^{6}A methylation-mediated *HMOX1* and *STEAP3* may be important regulators of adipocyte metabolism in muscle, implying that m^{6}A-induced ferroptosis may be a new target for regulating chicken IMF metabolism.

By analyzing the functional roles of DMGs in breast muscle at different developmental stages, it was revealed that hyper- and hypomethylated DMGs were primarily involved in protein and kinase activity regulation, actin binding, transcriptional regulation, and various energy metabolic processes. We identified that leiomodin-2 (***LMOD2***) is differentially expressed during breast muscle development and that its m^{6}A level is consistently downregulated. *LMOD2* is a protein in striated muscle cells that can bind to actin and participate in the formation of thin filaments (Kiss et al., 2020). *LMOD2* is only expressed in skeletal muscle and the myocardium, performing the similar function of lengthening thin filaments (Conley et al., 2001; Tsukada et al., 2010). String database exploration revealed that *LMOD2* functions similarly to muscle development-related genes (*CSRP3* and *MYL2*) and can regulate myofiber development, muscle contraction, and actin binding. *LMOD2* and *CSRP3* were identified as key genes regulating breast muscle development in yellow broilers, consistent with Li et al. (2020). It has been established that *CSRP3*, mainly expressed in skeletal muscle and myocardium, is an important cofactor in the initiation and maintenance of muscle-specific genes (Kong et al., 1997; Barash et al.,

2005) and can also be used as a functional candidate gene for pork quality regulation (Xu et al., 2010). IMF deposition results from adipocyte action mediated by complex gene regulatory networks in muscle. Therefore, the m^{6}A-modified gene *LMOD2* during muscle development may be a key candidate gene for regulating IMF metabolism.

Based on the m^{6}A methylation and gene expression association analysis results, 8 stage-specific DMGs (*HOGA1, MYH1F, LRRC66, TEKT1, DHX58, PPM1K, ANKRD2*, and *SACS*) were identified. The catabolic process of glycerol-3-phosphate and various amino acids was aided by 4-hydroxy-2-oxoglutarate aldolase 1 (***HOGA1***). *HOGA1* inhibition can significantly downregulate the expression of *PPARγ, C/EBPα, AP2, CD36*, and adiponectin during mouse adipocyte differentiation, inhibiting intracellular fat deposition (Kim et al., 2022). Protein phosphatase, Mg^{2+}/Mn^{2+}-dependent 1K (***PPM1K***), has mitochondrial pyruvate dehydrogenase activity and is a key enzyme in the catabolism of branched-chain amino acids (Knapik-Czajka et al., 2021). Myosin, heavy chain 1f (***MYH1F***), which is highly expressed in chicken skeletal muscle and involved in myogenesis processes, has been well characterized in regulating skeletal muscle contraction and actin binding (Ren et al., 2022). Ankyrin repeat domain-containing protein 2 (***ANKRD2***) functions as a transcriptional regulator in myogenesis-related processes. It is important in skeletal muscle development in pigs (Xu et al., 2018) and myofiber-type conversion in chickens (Stamenkovic et al., 2020). In summary, various amino acids in muscle and adipose tissue can differentially regulate the activity and gene expression of enzymes involved in fat metabolism and positively regulate muscle proteins and fatty acid synthesis. This process is also associated with mitochondrial-mediated energy metabolism. Therefore, the m^{6}A modification-mediated *HOGA1, PPM1K, MYH1F*, and *ANKRD2* may be potential candidate genes for regulating IMF-specific deposition, and their methylation modification activity may be associated with multiple functional activities during muscle biogenesis, including amino acid anabolism, protein and transcription factor activity regulation, and cell energy metabolism.

CONCLUSIONS

In conclusion, the present study examined the m^{6}A methylation modification patterns in Jingyuan chicken's breast muscle tissues during the growing period, sexual maturity, and marketing ages. Functional enrichment analysis of DMGs indicated that m^{6}A modification is critical in regulating the expression of genes related to IMF metabolism. Identifying m^{6}A-induced ferroptosis in breast muscle tissue may point to a new target for muscle adipogenesis. Further investigation revealed that *LMOD2* and its multiple m^{6}A negatively regulated DMGs are potential regulators of muscle fat anabolism. The findings of the present study lay a solid foundation for future investigation into the potential role of m^{6}A modification in regulating chicken IMF deposition.

ACKNOWLEDGMENTS

This study was supported by the Key R&D Program of the Ningxia Hui Autonomous Region (2022BBF02034).

DISCLOSURES

The authors declare no conflicts of interest.

SUPPLEMENTARY MATERIALS

Supplementary material associated with this article can be found in the online version at doi:10.1016/j.psj.2023.102793.

REFERENCES

Bailey, T. L., M. Boden, F. A. Buske, M. Frith, C. E. Grant, L. Clementi, J. Y. Ren, W. W. Li, and W. S. Noble. 2009. MEME SUITE: tools for motif discovery and searching. Nucleic Acids Res. 37:W202–W208.

Barash, I. A., L. Mathew, M. Lahey, M. L. Greaser, and R. L. Lieber. 2005. Muscle LIM protein plays both structural and functional roles in skeletal muscle. Am. J. Physiol. Cell Physiol. 289:C1312–C1320.

Cesar, A. S., L. C. A. Regitano, J. E. Koltes, E. R. Fritz-Waters, D. P. D. Lanna, G. Gasparin, G. B. Mourão, P. S. N. Oliveira, J. M. Reecy, and L. L. Coutinho. 2015. Putative regulatory factors associated with intramuscular fat content. PLoS One 10:e0128350.

Chen, R. N., K. Liao, H. R. Liao, L. Zhang, H. X. Zhao, and J. Sun. 2023. Screening and functional validation of lipid metabolism-related lncRNA-46546 based on the transcriptome analysis of early embryonic muscle tissue in chicken. Anim. Biosci. 36:175–190.

Chen, J. L., J. Wen, S. B. Wang, G. P. Zhao, M. Q. Zheng, and X. H. Li. 2005. Studies on the characteristics of deposition of chicken IMP and IMF. Acta Vet. Zootech. Sin. 36:843–845.

Chen, L. X., N. Wu, L. Kennedy, H. Francis, L. Ceci, T. Zhou, N. Samala, K. Kyritsi, C. Wu, A. Sybenga, B. Ekser, W. Dar, C. Atkins, V. Meadows, S. Glase, and G. Alpini. 2021. Inhibition of secretin/secretin receptor axis ameliorates NAFLD phenotypes. Hepatology 74:1845–1863.

Chen, S. F., Y. Q. Zhou, Y. R. Chen, and J. Gu. 2018. fastp: an ultra-fast all-in-one FASTQ preprocessor. Bioinformatics 34:i884–i890.

Cheng, J., L. Wang, S. S. Wang, R. Chen, T. Zhang, H. D. Ma, H. Z. Lu, and G. Q. Yuan. 2021. Transcriptomic analysis of thigh muscle of Lueyang black-bone chicken in free-range and caged feeding. Anim. Biotechnol. 1–11.

Conley, C. A., K. L. Fritz-Six, A. Almenar-Queralt, and V. M. Fowler. 2001. Leiomodins: larger members of the tropomodulin (Tmod) gene family. Genomics 73:127–139.

Cui, H. X., M. Q. Zheng, G. P. Zhao, R. R. Liu, and J. Wen. 2018. Identification of differentially expressed genes and pathways for intramuscular fat metabolism between breast and thigh tissues of chickens. BMC Genom. 19:55.

Davis, T. A., A. Suryawan, R. A. Orellana, H. V. Nguyen, and M. L. Fiorotto. 2008. Postnatal ontogeny of skeletal muscle protein synthesis in pigs. J. Anim. Sci. 86:E13–E18.

Ding, H. R., S. J. Chen, X. H. Pan, X. S. Dai, G. H. Pan, Z. Li, X. D. Mai, Y. Tian, S. S. Zhang, B. D. Liu, G. C. Cao, Z. C. Yao, X. P. Yao, L. Gao, L. Yang, X. Y. Chen, J. Sun, H. Chen, M. L. Han, Y. L. Yi, G. H. Xu, H. J. Li, W. D. Wu, Z. Chen, J. C. Lin, L. P. Xiang, J. Hu, Y. Lu, X. Zhu, and L. W. Xie. 2021. Transferrin receptor 1 ablation in satellite cells impedes skeletal

muscle regeneration through activation of ferroptosis. J. Cachexia Sarcopenia Muscle 12:746–768.
Dominissini, D., S. Moshitch-Moshkovitz, S. Schwartz, M. Salmon-Divon, L. Ungar, S. Osenberg, K. Cesarkas, J. Jacob-Hirsch, N. Amariglio, M. Kupiec, R. Sorek, and G. Rechavi. 2012. Topology of the human and mouse m6A RNA methylomes revealed by m6A-seq. Nature 485:201–206.
Fan, Y., C. S. Zhang, and G. Y. Zhu. 2019. Profiling of RNA N6-methyladenosine methylation during follicle selection in chicken ovary. Poult. Sci. 98:6117–6124.
Frank, D., S. T. Joo, and R. Warner. 2016. Consumer acceptability of intramuscular fat. Korean J. Food Sci. Anim. Resour. 36:699–708.
Frye, M., B. T. Harada, M. Behm, and C. He. 2018. RNA modifications modulate gene expression during development. Science 361:1346–1349.
Guo, S. K., X. D. Wang, M. L. Cao, X. Y. Wu, L. Xiong, P. J. Bao, M. Chu, C. N. Liang, P. Yan, J. Pei, and X. Guo. 2022. The transcriptome-wide N6-methyladenosine (m^6A) map profiling reveals the regulatory role of m6A in the yak ovary. BMC Genom. 23:358.
Heinz, S., C. Benner, N. Spann, E. Bertolino, Y. C. Lin, P. Laslo, J. X. Cheng, C. Murre, H. Singh, and C. K. Glass. 2010. Simple combinations of lineage-determining transcription factors prime cis-regulatory elements required for macrophage and B cell identities. Mol. Cell 38:576–589.
Hocquette, J. F., F. Gondret, E. Baéza, F. Médale, C. Jurie, and D. W. Pethick. 2010. Intramuscular fat content in meat-producing animals: development, genetic and nutritional control, and identification of putative markers. Animal 4:303–319.
Huh, J. Y., S. M. Reilly, M. Abu-Odeh, A. N. Murphy, S. K. Mahata, J. Zhang, Y. Cho, J. B. Seo, C. W. Hung, C. R. Green, C. M. Metallo, and A. R. Saltiel. 2020. TANK-binding kinase 1 regulates the localization of acyl-CoA synthetase ACSL1 to control hepatic fatty acid oxidation. Cell Metab. 32:1012–1027.
Jiang, C. D., P. Shi, S. Li, R. R. Dong, J. W. Tian, J. Wei, and S. Luo. 2010. Gene expression profiling of skeletal muscle of nursing piglets. Int. J. Biol. Sci. 6:627–638.
Jiang, X., B. R. Stockwell, and M. Conrad. 2021. Ferroptosis: mechanisms, biology and role in disease. Nat. Rev. Mol. Cell. Biol. 22:266–282.
Jiang, Q., B. F. Sun, Q. Liu, M. Cai, R. F. Wu, F. Q. Wang, Y. X. Yao, Y. Z. Wang, and X. X. Wang. 2019. MTCH2 promotes adipogenesis in intramuscular preadipocytes via an m6A-YTHDF1-dependent mechanism. FASEB J. 33:2971–2981.
Katsumata, M. 2011. Promotion of intramuscular fat accumulation in porcine muscle by nutritional regulation. Anim. Sci. J. 82:17–25.
Kim, D., B. Langmead, and S. L. Salzberg. 2015. HISAT: a fast spliced aligner with low memory requirements. Nat. Methods 12:357–360.
Kim, M., K. W. Park, Y. Ahn, E. B. Lim, S. H. Kwak, A. Randy, N. J. Song, K. S. Park, C. W. Nho, and Y. S. Cho. 2022. Genetic association-based functional analysis detects HOGA1 as a potential gene involved in fat accumulation. Front. Genet. 13:951025.
Kiss, B., J. Gohlke, P. Tonino, Z. Hourani, J. Kol, J. Strom, O. Alekhina, J. E. Smith 3rd, C. Ottenheijm, C. Gregorio, and H. Granzier. 2020. Nebulin and Lmod2 are critical for specifying thin-filament length in skeletal muscle. Sci. Adv. 6:eabc1992.
Knapik-Czajka, M., M. Jurczyk, J. Bieleń, V. Aleksandrovych, A. Gawędzka, P. Stach P, J. Drąg, and K. Gil. 2021. Effect of 5-fluorouracil on branched-chain α-keto acid dehydrogenase (BCKDH) complex in rat's heart. Folia Med. Cracov 61:121–129.
Kong, Y., M. J. Flick, A. J. Kudla, and S. F. Konieczny. 1997. Muscle LIM protein promotes myogenesis by enhancing the activity of MyoD. Mol. Cell. Biol. 17:4750–4760.
Laukkanen, O., J. Pihlajamäki, J. Lindström, J. Eriksson, T. T. Valle, H. Hämäläinen, P. Ilanne-Parikka, S. Keinänen-Kiukaanniemi, J. Tuomilehto, M. Uusitupa, and M. Laakso. 2004. Finnish Diabetes Prevention Study Group. 2004. Common polymorphisms in the genes regulating the early insulin signalling pathway: effects on weight change and the conversion from impaired glucose tolerance to Type 2 diabetes. The Finnish diabetes prevention study. Diabetologia 47:871–877.
Le Bihan-Duval, E., C. Berri, E. Baeza, N. Millet, and C. Beaumont. 2001. Estimation of the genetic parameters of meat characteristics and of their genetic correlations with growth and body composition in an experimental broiler line. Poult. Sci. 80:839–843.
Lee, H., S. Y. Bao, Y. Z. Qian, S. Geula, J. Leslie, C. L. Zhang, J. H. Hanna, and L. Ding. 2019. Stage-specific requirement for Mettl3-dependent m6A mRNA methylation during haematopoietic stem cell differentiation. Nat. Cell Biol. 21:700–709.
Li, D. F., Z. X. Pan, K. Zhang, M. L. Yu, D. B. Yu, Y. L. Lu, J. T. Wang, J. Zhang, K. N. Zhang, and W. X. Du. 2020. Identification of the differentially expressed genes of muscle growth and intramuscular fat metabolism in the development stage of Yellow Broilers. Genes (Basel) 11:244.
Luo, G. Z., A. MacQueen, G. Q. Zheng, H. C. Duan, L. C. Dore, Z. K. Lu, J. Liu, K. Chen, G. F. Jia, J. Bergelson, and C. He. 2014. Unique features of the m6A methylome in Arabidopsis thaliana. Nat. Commun. 5:5630.
Luo, G., S. H. Wang, Y. T. Ai, J. P. Li, and Z. J. Ren. 2022. N6-methyladenosine methylome profiling of muscle and adipose tissues reveals methylase-mRNA metabolic regulatory networks in fat deposition of Rex rabbits. Biology (Basel) 11:944.
Mariman, E. C., and P. Wang. 2010. Adipocyte extracellular matrix composition, dynamics and role in obesity. Cell. Mol. Life Sci. 67:1277–1292.
Meng, J., Z. L. Lu, H. Liu, L. Zhang, S. W. Zhang, Y. D. Chen, M. K. Rao, and Y. F. Huang. 2014. A protocol for RNA methylation differential analysis with MeRIP-Seq data and exomePeak R/Bioconductor package. Methods 69:274–281.
Merkestein, M., S. Laber, F. McMurray, D. Andrew, G. Sachse, J. Sanderson, M. Li, S. Usher, D. Sellayah, F. M. Ashcroft, and R. D. Cox. 2015. FTO influences adipogenesis by regulating mitotic clonal expansion. Nat. Commun. 6:6792.
Meyer, K. D., Y. Saletore, P. Zumbo, O. Elemento, C. E. Mason, and S. R. Jaffrey. 2012. Comprehensive analysis of mRNA methylation reveals enrichment in 3′ UTRs and near stop codons. Cell 149:1635–1646.
Moreno-Navarrete, J. M., F. Ortega, A. Rodríguez, J. Latorre, S. Becerril, M. Sabater-Masdeu, W. Ricart, G. Frühbeck, and J. M. Fernández-Real. 2017. HMOX1 as a marker of iron excess-induced adipose tissue dysfunction, affecting glucose uptake and respiratory capacity in human adipocytes. Diabetologia 60:915–926.
Ohgami, R. S., D. R. Campagna, E. L. Greer, B. Antiochos, A. McDonald, J. Chen, J. J. Sharp, Y. Fujiwara, J. E. Barker, and M. D. Fleming. 2005. Identification of a ferrireductase required for efficient transferrin-dependent iron uptake in erythroid cells. Nat. Genet. 37:1264–1269.
Ohgami, R. S., D. R. Campagna, A. McDonald, and M. D. Fleming. 2006. The steap proteins are metalloreductases. Blood 108:1388–1394.
Ou, Z. M., Y. Y. Shi, Q. Q. Li, Y. Wu, and F. F. Chen. 2022. Effects of sex on the muscle development and meat composition in Wuliangshan black-bone chickens. Animals (Basel) 12:2565.
Park, E. J., O. J. Koo, and B. C. Lee. 2015. Overexpressed human heme oxygenase-1 decreases adipogenesis in pigs and porcine adipose-derived stem cells. Biochem. Biophys. Res. Commun. 467:935–940.
Pertea, M., G. M. Pertea, C. M. Antonescu, T. C. Chang, J. T. Mendell, and S. L. Salzberg. 2015. StringTie enables improved reconstruction of a transcriptome from RNA-seq reads. Nat. Biotechnol. 33:290–295.
Petracci, M., and C. Cavani. 2012. Muscle growth and poultry meat quality issues. Nutrients 4:1–12.
Ren, P., M. Y. Chen, J. J. Li, Z. Z. Lin, C. W. Yang, C. L. Yu, D. H. Zhang, and Y. P. Liu. 2022. MYH1F promotes the proliferation and differentiation of chicken skeletal muscle satellite cells into myotubes. Anim. Biotechnol. 1–11.
Robinson, M. D., D. J. McCarthy, and G. K. Smyth. 2010. edgeR: a bioconductor package for differential expression analysis of digital gene expression data. Bioinformatics 26:139–140.
Roundtree, I. A., M. E. Evans, T. Pan, and C. He. 2017. Dynamic RNA modifications in gene expression regulation. Cell 169:1187–1200.
Ruan, F. K., J. Zeng, H. Y. Yin, S. W. Jiang, X. S. Cao, N. Y. Zheng, C. S. Han, C. C. Zhang, Z. H. Zuo, and C. Y. He. 2021. RNA m6A modification alteration by black phosphorus quantum dots

regulates cell ferroptosis: implications for nanotoxicological assessment. Small Methods 5:e2001045.
Saltiel, A. R., and J. E. Pessin. 2002. Insulin signaling pathways in time and space. Trends Cell Biol. 12:65–71.
Sastry, S. K., and K. Burridge. 2000. Focal adhesions: a nexus for intracellular signaling and cytoskeletal dynamics. Exp. Cell Res. 261:25–36.
Shen, M., Y. J. Li, Y. Q. Wang, J. J. Shao, F. Zhang, G. P. Yin, A. P. Chen, Z. L. Zhang, and S. Z. Zheng. 2021. N^6-methyladenosine modification regulates ferroptosis through autophagy signaling pathway in hepatic stellate cells. Redox Biol. 47:102151.
Song, T. X., Y. Yang, S. W. Jiang, and J. Peng. 2020. Novel insights into adipogenesis from the perspective of transcriptional and RNA N6-methyladenosine-mediated post-transcriptional regulation. Adv. Sci. (Weinh.) 7:2001563.
Soto-Avellaneda, A., and B. E. Morrison. 2020. Signaling and other functions of lipids in autophagy: a review. Lipids Health Dis. 19:214.
Stamenkovic, N., J. Jasnic, M. Novkovic, E. Milosevic, S. Boskovic, A. Koji, K. Popic, M. Stankovic, Y. Wang, S. Milenkovic, D. Radojkovi, G. Ma, and S. Kojic. 2020. Cloning and expression profiling of muscle regulator ANKRD2 in domestic chicken Gallus gallus. Histochem. Cell Biol. 154:383–396.
Stockwell, B. R. 2022. Ferroptosis turns 10: emerging mechanisms, physiological functions, and therapeutic applications. Cell 185:2401–2421.
Tsukada, T., C. T. Pappas, N. Moroz, P. B. Antin, A. S. Kostyukova, and C. C. Gregorio. 2010. Leiomodin-2 is an antagonist of tropomodulin-1 at the pointed end of the thin filaments in cardiac muscle. J. Cell Sci. 123:3136–3145.
Wang, Y., D. Botolin, J. H. Xu, B. Christian, E. Mitchell, B. Jayaprakasam, M. G. Nair, J. M. Peters, J. V. Busik, L. K. Olson, and D. B. Jump. 2006. Regulation of hepatic fatty acid elongase and desaturase expression in diabetes and obesity. J. Lipid Res. 47:2028–2041.
Wang, K., M. Y. Li, and H. Hakonarson. 2010. ANNOVAR: functional annotation of genetic variants from high-throughput sequencing data. Nucleic Acids Res. 38:e164.
Wang, Y. S., W. X. Tian, and R. Y. Hsu. 1984. Hybridization studies of chicken liver fatty acid synthetase. Evidence for the participation in palmitate synthesis of cysteine and phosphopantetheine sulfhydryl groups on adjacent subunits. J. Biol. Chem. 259:13644–13647.
Wang, Z., D. D. Wang, K. R. Jiang, Y. L. Guo, Z. J. Li, R. R. Jiang, R. L. Han, G. X. Li, Y. D. Tian, H. Li, X. T. Kang, and X. J. Liu. 2021. A comprehensive proteome and acetyl-proteome atlas reveals molecular mechanisms adapting to the physiological changes from pre-laying to peak-laying stage in liver of hens (Gallus gallus). Front. Vet. Sci. 8:700669.
Wang, X. X., L. N. Zhu, J. Q. Chen, and Y. Z. Wang. 2015. mRNA m^6A methylation downregulates adipogenesis in porcine adipocytes. Biochem. Biophys. Res. Commun. 459:201–207.
Wu, W., J. Feng, D. H. Jiang, X. H. Zhou, Q. Jiang, M. Cai, X. X. Wang, T. Z. Shan, and Y. Z. Wang. 2017. AMPK regulates lipid accumulation in skeletal muscle cells through FTO-dependent demethylation of N6-methyladenosine. Sci. Rep. 7:41606.
Xu, X. W., H. F. Qiu, Z. Q. Du, B. Fan, R. M. Fothschild, F. Yuan, and B. Liu. 2010. Porcine CSRP3: polymorphism and association analyses with meat quality traits and comparative analyses with CSRP1 and CSRP2. Mol. Biol. Rep. 37:451–459.
Xu, J. G., C. L. Wang, E. Jin, Y. F. Gu, S. H. Li, and Q. G. Li. 2018. Identification of differentially expressed genes in longissimus dorsi muscle between Wei and Yorkshire pigs using RNA sequencing. Genes Genom. 40:413–421.
Xu, T. S., Z. J. Xu, L. Z. Lu, T. Zeng, L. H. Gu, Y. Z. Huang, S. J. Zhang, P. Yang, Y. F. Wen, D. J. Lin, M. P. Xing, L. L. Huang, G. J. Liu, Z. Chao, and W. P. Sun. 2021. Transcriptome-wide study revealed m6A regulation of embryonic muscle development in Dingan goose (Anser cygnoides orientalis). BMC Genom. 22:270.
Yang, Y., P. J. Hsu, Y. S. Chen, and Y. G. Yang. 2018. Dynamic transcriptomic m6A decoration: writers, erasers, readers and functions in RNA metabolism. Cell Res. 28:616–624.
Yang, M. M., B. W. Hu, D. L. Sun, C. B. Zhao, H. H. Wei, D. J. Li, Z. Y. Liao, Y. X. Zhao, J. P. Liang, M. Q. Shi, Q. B. Luo, Q. H. Nie, X. Q. Zhang, D. X. Zhang, and H. M. Li. 2022. Growth hormone receptor gene influences mitochondrial function and chicken lipid metabolism by AMPK-PGC1α-PPAR signaling pathway. BMC Genom. 23:219.
Zhang, Y. F., C. N. Liang, X. Y. Wu, J. Pei, X. Guo, M. Chu, X. Z. Ding, P. J. Bao, Q. Kalwar, and P. Yan. 2021. Integrated study of transcriptome-wide m6A methylome reveals novel insights into the character and function of m6A methylation during Yak adipocyte differentiation. Front. Cell Dev. Biol. 9:689067.
Zhao, G. P., J. L. Chen, M. Q. Zheng, J. Wen, and Y. Zhang. 2007. Correlated responses to selection for increased intramuscular fat in a Chinese quality chicken line. Poult. Sci. 86:2309–2314.
Zhao, B. S., I. A. Roundtree, and C. He. 2017. Post-transcriptional gene regulation by mRNA modifications. Nat. Rev. Mol. Cell. Biol. 18:31–42.
Zhao, X., Y. Yang, B. F. Sun, Y. Shi, X. Yang, W. Xiao, Y. J. Hao, X. L. Ping, Y. S. Chen, W. J. Wang, K. X. Jin, X. Wang, C. M. Huang, Y. Fu, X. M. Ge, S. H. Song, H. S. Jeong, H. Yanagisawa, Y. Niu, G. F. Jia, W. Wu, W. M. Tong, A. Okamoto, C. He, J. M. Rendtlew Danielsen, X. J. Wang, and Y. G. Yang. 2014. FTO-dependent demethylation of N6-methyladenosine regulates mRNA splicing and is required for adipogenesis. Cell Res. 24:1403–1419.